Fluid interactions with metafilms/metasurfaces for tuning, sensing, and microwave-assisted chemical processes

Joshua A. Gordon, Christopher L. Holloway, James Booth, Sung Kim, Yu Wang, James Baker-Jarvis, and David R. Novotny
National Institute of Standards and Technology, Electromagnetics Division, Boulder, Colorado 80305, USA
(Received 16 February 2011; revised manuscript received 31 March 2011; published 25 May 2011)

In this paper we demonstrate tunability of a metasurface, which is the two-dimensional equivalent of a metamaterial, also referred to as a metafilm, by changing the permittivity in a continuous flow channel that interacts with the metasurface. Numerical simulations and experimental results are presented for a metasurface consisting of metallic electric-field coupled resonators operating in *S* band near 3.6 GHz. The localization and enhancement of the electric field in the metasurface that interacts with the fluid channels is explored as a means for implementing and aiding microwave assisted chemical processes. Applications of such continuous flow tunable metasurfaces are discussed.

DOI: 10.1103/PhysRevB.83.205130 PACS number(s): 78.70.Gq, 41.20.−q, 74.25.N−, 77.84.Nh

I. INTRODUCTION

Metamaterials are commonly engineered by arranging a large number of small scatterers in a regular array throughout a region of space to obtain a desirable bulk electromagnetic behavior.[1–3] This concept can be extended by arranging electrically small scatterers into a two-dimensional pattern at a surface or interface (see Fig. 1). This surface version of a metamaterial is called a metafilm or metasurface.[4,5] These metafilms are also referred to in the literature as metasurfaces and/or single-layer metamaterials. The simplicity of metasurfaces makes them attractive alternatives to three-dimensional (3D) metamaterials for many applications. Several unique properties of metasurfaces have been reported, including sub-half-wavelength cavities,[6] guiding waves,[7] and resonant metasurfaces.[8]

Previous published work on fluid tunable frequency selective surfaces (FSSs)[9–11] focuses on tuning the band-pass response of an array of *nonresonant* structures. In contrast, here we investigate the interaction of a metafilm/metasurface array of *highly resonant* structures with a fluid. We demonstrate experimentally the frequency tuning of a metasurface through interaction with a dielectric fluid, such as de-ionized water, and explore using a metasurface to concentrate and enhance the delivery and interaction of electromagnetic energy with a fluidic systems. Such metasurface/fluid interactions may have potential significant applications for dynamic frequency tuning as well as sensing, process monitoring, and controlling *in vivo* microwave interactions during a chemical process.[12–14]

II. ANALYSIS OF METASURFACES

Similar to a metamaterial, the behavior of a metasurface can be characterized by the electric and magnetic polarizabilities of its constituent scatterers. The most convenient method to analyze metamaterials is with effective-medium theory. However, because the effective material properties are not uniquely defined for a metasurface, a more appropriate characterization of metasurfaces is given by generalized sheet transition conditions (GSTCs).[4] The GSTCs relating the electromagnetic fields at a metasurface interface were given in Ref. 5 and can be expressed in the form (assuming $e^{j\omega t}$ time dependence)

$$\vec{a}_z \times \vec{H}|_{z=0^-}^{0^+} = j\omega\varepsilon_0 \overleftrightarrow{\chi}_{ES} \cdot \vec{E}_{t,av}|_{z=0} - \vec{a}_z \times \nabla_t \left[\chi_{MS}^{zz} H_{z,av}\right]_{z=0}, \quad (1)$$

$$\vec{E}|_{z=0^-}^{0^+} \times \vec{a}_z = j\omega\mu_0 \overleftrightarrow{\chi}_{MS} \cdot \vec{H}_{t,av}|_{z=0} - \nabla_t \left[\chi_{ES}^{zz} E_{z,av}\right]_{z=0} \times \vec{a}_z, \quad (2)$$

where $\vec{a}_z$ is the surface normal, and $\vec{E}_t$ and $\vec{H}_t$ are the tangential components of the electric and magnetic field, respectively, where the subscript "*av*" represents the average of the field quantity on either side of the metasurface. The parameters $\overleftrightarrow{\chi}_{ES}$ and $\overleftrightarrow{\chi}_{MS}$ are the dyadic effective surface electric and magnetic susceptibilities, which have units of meters and are related to the electric and magnetic polarizability of the scatterers that compose the metasurface. For simplicity, we consider here only the case where the scatterers have sufficient symmetry such that the surface susceptibility dyadics are diagonal, and are given by

$$\overleftrightarrow{\chi}_{ES} = \chi_{ES}^{xx}\vec{a}_x\vec{a}_x + \chi_{ES}^{YY}\vec{a}_y\vec{a}_y + \chi_{ES}^{zz}\vec{a}_z\vec{a}_z, \quad (3)$$

$$\overleftrightarrow{\chi}_{MS} = \chi_{MS}^{xx}\vec{a}_x\vec{a}_x + \chi_{MS}^{YY}\vec{a}_y\vec{a}_y + \chi_{MS}^{zz}\vec{a}_z\vec{a}_z, \quad (4)$$

The relationship between these surface susceptibilities and the electric and magnetic polarizabilities of the individual scatterer that compose the metasurface were discussed in Refs. 5 and 15. Using these GSTCs, the reflection and transmission properties of a metasurface are investigated in Ref. 15, where it is shown that with the right choice of scatterer polarizabilities (and in turn the right choice of the surface susceptibilities), total reflection and total transmission properties can be realized. For total reflection, the following conditions must be met:

$$\begin{aligned} k_0^2\chi_{MS}^{xx}\left[\chi_{ES}^{yy} - \chi_{MS}^{zz}\sin(\theta)^2\right] &= 4 \quad \text{for TE,} \\ k_0^2\chi_{ES}^{xx}\left[\chi_{MS}^{yy} - \chi_{ES}^{zz}\sin(\theta)^2\right] &= 4 \quad \text{for TM} \end{aligned} \quad (5)$$

and for total transmission the following conditions must be met:

$$\begin{aligned} \chi_{ES}^{yy} + \chi_{MS}^{xx}\cos(\theta)^2 - \chi_{MS}^{zz}\sin(\theta)^2 &= 0 \quad \text{for TE,} \\ \chi_{MS}^{yy} + \chi_{ES}^{xx}\cos(\theta)^2 - \chi_{ES}^{zz}\sin(\theta)^2 &= 0 \quad \text{for TM,} \end{aligned} \quad (6)$$

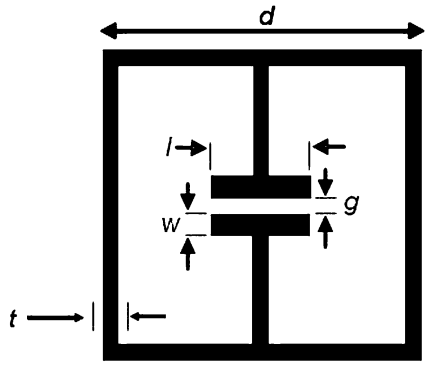

FIG. 1. Electric-field coupled resonator used in metasurface design.

where TE and TM are with respect to the z axis that is normal to the metasurface, θ is the angle of incidence measured from the surface normal of the metasurface, and k_0 is the free-space wave number. In this paper, we present experimental results demonstrating the ability to tune the frequencies over which reflection and transmission occur for a metasurface by changing the polarizability of the inclusions via a microfluidic channel.

A few comments are needed on (i) the difference between a metamaterial and a conventional photonic band gap (PBG) structure and, in turn, (ii) the difference between a metasurface and a conventional frequency selective surface (FSS). We began our discussion with metamaterial concepts that are extended to metasurfaces. To this end, it is important to understand the behavior for various frequency ranges or length scales of a periodic composite material.

First, consider the case when the wavelength approaches the period of a periodic structure. In this region, the electromagnetic field interaction with the periodic structure is very involved. Scattering is the mechanism for the field behavior and we cannot think of the composite material behaving like an effective medium. When the wavelength approaches the period, higher-order Floquet-Bloch modes must be considered, and as such FSS and PBG are the predominate applications in this region, and one typically does not refer to these materials as metamaterials or metasurfaces. This causes unique characteristics in the field behavior and results in unique applications. High-frequency applications of periodic structures have been given various names throughout the literature. In recent years, 2D high-frequency periodic structures have been given the name frequency selective surfaces (FSSs)[16] (historically known as periodic gratings) and high-frequency three-dimensional periodic materials have been given the name photonic band gap (PBG) materials,[17] although a more appropriate term given to these three-dimensional periodic materials at microwave frequencies is electromagnetic band gap (EBG) materials. FSS and PBG/ EBG materials have similar characteristics in that, at certain frequencies, the FSS and PBG/EBG block or stop the propagation of EM waves either across the surface or through the materials. The frequency bands where this occurs are referred to as stopbands. At other frequencies the periodic structure allows energy to propagate through the structure; these frequency bands are referred to as passbands.

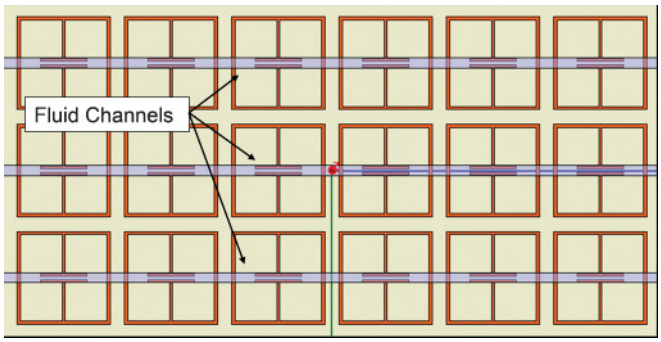

FIG. 2. (Color online) Microfluidic tunable metasurface.

The second case (period smaller than half the wavelength) corresponds to a region where the scatterers are designed in such a manner (either the shape or bulk material properties) such that the scatterers themselves can resonate. When this occurs, a new class of manmade materials (metamaterials) can be realized that can have a broad range of unique behaviors commonly not found in nature, for example, double negative materials (DNG), or near zero-index materials. Similar behavior will be present for scatterers in a 2D surface (the metasurface). For a 2D array of scatterers, the region where the wavelength approaches the period of the structure corresponds to resonances associated with the periodicity of the scatterers. The conventional FSS operates far into this region. On the other hand, when we talk about metafilms or metasurfaces, we are referring to an array of scatterers that fall into the second case (period smaller than half the wavelength); that is, resonances of the surface that are associated with the resonances of the scatterers, and not associated with the periodicity of the array (i.e., a nonconventional FSS).

III. DESIGN AND SIMULATION OF METASURFACE

In designing the metasurface for these investigations it is required that there is strong interaction between the fluid in the microfluidic channel and the structure. To accomplish this, inclusions were selected that would allow for direct interaction between the local fields excited in the inclusion by the incident wave and the fluid channel. Figure 1 shows the electric-field coupled inclusion that was chosen for our metasurface design. This type of inclusion is easily excited by the electric field of the incident wave allowing the plane of the inclusions to be oriented parallel to the plane of the metasurface. Being able to orient the inclusion in the plane of the metasurface has several attractive features: (i) it is consistent with the planar fabrication techniques used for microwave circuits and Polydimethylsiloxane (PDMS) microfluid channels,[18] (ii) it allows the capacitive gaps for each inclusion to be simultaneously aligned to each other as well as the fluid channel, thereby allowing multiple inclusions to share the same fluidic channel path, and (iii) it allows the fluid channels to be in direct contact with the capacitive gaps of the inclusions, which facilitates strong coupling of the fluid channels to the electric field excited in the capacitive gaps.

Because the fluid channels strongly interact with the fringe fields in the gaps, a change in the permittivity of the fluid will affect the capacitive response of each inclusion and, in

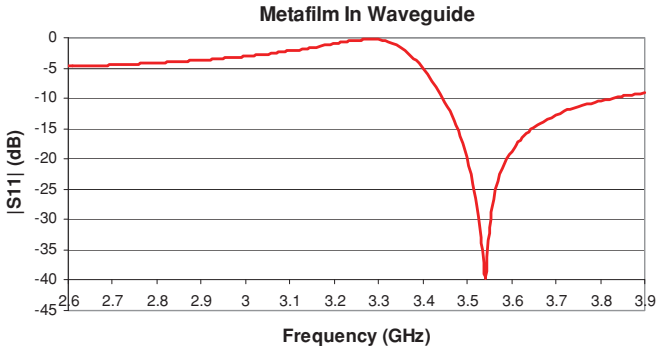

FIG. 3. (Color online) Simulated resonant behavior of a 3×6 metasurface array composed of electric-field-coupled resonators inside an *S*-band waveguide.

turn, the polarizability. This results in an effective electric and magnetic surface susceptibility $\overleftrightarrow{\chi}_{ES}$ and $\overleftrightarrow{\chi}_{MS}$, which can be altered by changing the permittivity of the fluid in the channels. As can be seen from Eqs. (5) and (6), changes in the sheet susceptibilities will, in general, affect the reflection and transmission properties of the metasurface. Changing the electrical properties of the fluid in the channels therefore provides a means for tuning the resonances of the metasurface. This same tuning mechanism may be used inversely as a means to monitor and detect changes of the electrical properties of the fluid in the channels. A diagram of the fluid channel coupled metasurface is shown in Fig. 2 above.

The simulations discussed here were performed using Ansoft HFSS (mention of this product is not an endorsement, but only serves to clarify the software used). The precision for the frequency sweep was set to a 10-MHz step size. The accuracy of the simulations was constrained by using an adaptive solution where the finite element mesh was continually refined until the maximum change in the magnitude of all the *S* parameters between simulation refinements was below 0.01.

In designing the metasurface structure, the resonant characteristics of an infinite array of identical electric-field coupled scatterers was first simulated. The infinite metasurface was simulated using Floquet mode analysis of a single inclusion with periodic boundary conditions and excited with an incident plane wave at the angle corresponding to that of the mode propagating in an *S* band waveguide at the desired resonant frequency. Using this infinite-array analysis, approximate design parameters for a single inclusion could then be determined for the desired operating frequency range in the *S* band. A full-wave simulation was then performed for a finite 3×6 array placed cross-sectionally inside a standard 7.2-cm $\times$ 3.4-cm perfect electric conductor *S* band waveguide to determine the response for the array interacting with the waveguide mode. A parametric simulation was then performed for the 3×6 array in the waveguide in order to optimize the inclusion design parameters for operation in the waveguide.

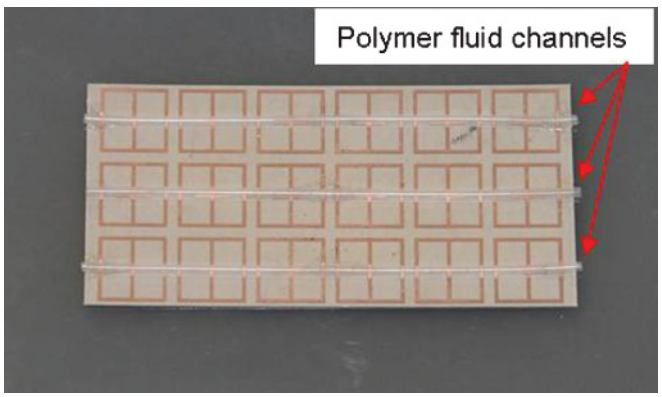

FIG. 4. (Color online) Microfluidic metasurface composed of a 3×6 array of electric-field coupled resonators fabricated from copper on Duroid® with three polymer tubing fluid channel sections.

Figure 3 shows $|S_{11}|$ simulation results for the 3×6 array inside the waveguide. The final design parameters were $t = w = 0.5$ mm, $d = 9.5$ mm, $l = 5$ mm, $g = 0.15$ mm, with an inclusion spacing period $= 11$ mm. The array was simulated as 17-μm-thick copper on a 0.508-mm-thick Duroid® substrate with relative permittivity, $\varepsilon = 2.94$. Behavior is observed where the metasurface passes through resonances near 3.29 GHz where the condition for total reflection is satisfied and also near 3.54 GHz where the condition for total transmission is satisfied [see Eqs. (5) and (6) above].

IV. EXPERIMEMTAL RESULTS OF A FLUID TUNABLE METASURFACE

The same 3×6 metasurface array structure that was simulated above was then fabricated from the Duroid® 6002 High Frequency Laminate with 17-μm-thick copper laminated to 0.508-mm-thick substrate and coupled to fluid channels to investigate tuning. Polymer tubing was used for fluid channels because of difficulty bonding and sealing PDMS fluid channels to the Duroid® substrate. The polymer fluid channels were bonded to the metasurface using cyanoacrylate based glue. A picture of the metasurface with polymer fluid channels bonded and aligned across the gaps of the inclusions is shown in Fig. 4. A gold metasurface array on a quartz substrate that was bonded to PDMS fluid channels was also tried. However, due to fabrication limitations, the gold could not be made thick enough and therefore the metal losses were too great to allow any resonance effect to be observed.

The 3×6 metasurface array was placed in a vertically oriented standard 7.2-cm $\times$ 3.4-cm rectangular *S*-band waveguide so that gravity acted parallel to the waveguide axis, and normal to the plane of the metasurface and fluid channel flow (see Fig. 5). The metasurface array was supported by a block of polystyrene foam that filled 2/3 of the waveguide so that the metasurface could be easily located in and removed from the waveguide in order to facilitate quick filling of the fluid channels. The input and output ports of the waveguide were then connected to a calibrated vector network analyzer.

Employing the TRL (through reflection line) calibration method,[19] we measured the scattering parameters of the waveguide over the frequency range 2.6–3.95 GHz. The measurement uncertainties in the reflection coefficient resulting from this calibration method are $\Delta |S_{11}| = 0.02$ (one standard deviation).[19]

S-parameter measurements with and without fluid in the channels were performed to determine the tuning of the transmission resonance. De-ionized (DI) water with a nominal relative permittivity of $\varepsilon = 76$ over the measurement

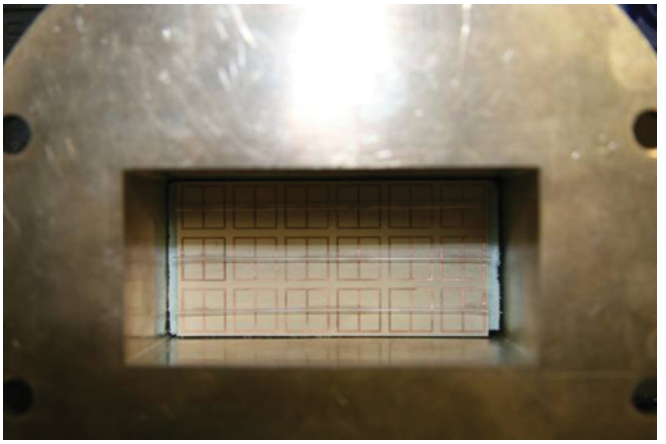

FIG. 5. (Color online) Experimental setup with the 3×6 array of electric-field coupled resonators fabricated from copper on Duroid® with three polymer tubing fluid channel sections placed in *S*-band waveguide.

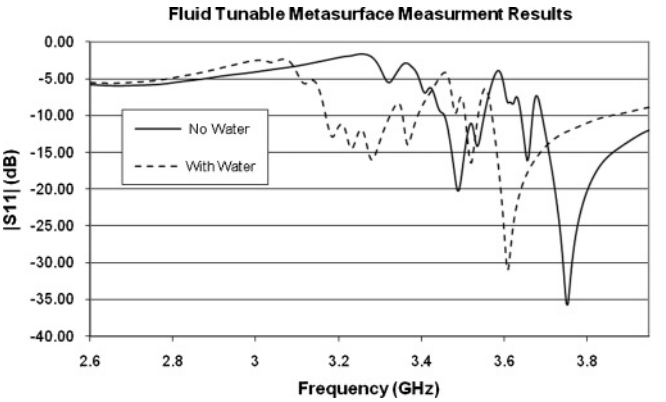

FIG. 6. Experimental results comparing $|S_{11}|$ for fluid channels empty (solid curve) and filled with DI water (dashed curve) over the *S* band from 2.6 to 3.95 GHz.

frequency range of 2.6–3.95 GHz was chosen to test the frequency tunability of the metasurface because of its ease of handling, low volatility, high dielectric constant, and low loss in the *S* band, and water is also a common dielectric background in many biological fluids. Fluid channels were manually filled using a syringe. Figure 5 shows the experimental setup with the metasurface inside the *S*-band waveguide.

Experimental results shown in Fig. 6 demonstrate tunability over a frequency range of 150 MHz. The dip in $|S_{11}|$ is clearly shifted from 3.75 GHz down to 3.6 GHz between the cases without and with water in the fluid channels, respectively (see Fig. 6). The disagreement between the positions of the resonance dip for the case without water compared to that of the simulated result in Fig. 3 above for the metasurface without fluid channels in a free-space-filled waveguide is due to inclusion fabrication errors.

These fabrication errors resulted in a discrepancy between the simulated inclusion dimensions and those actually fabricated. The overall effect of these fabrication errors was a lower resonance frequency. The additional oscillations observed in the experimental measurements are also a result of fabrication uniformity and periodicity errors of the inclusions as well as nonuniform perturbations across the metasurface due to errors in bonding the fluid channels. In the future, fabrication improvements will be explored to mitigate these errors. In addition to using fluids for specifically tuning microwave characteristics, the changes in resonance characteristics may also be used to monitor the process related to the changes in the fluid flowing in the channels, and have applications to manufacturing, industrial, biomedical, and chemical processes.

V. APPLICATION OF METASURFACES TO MICROWAVE-ASSISTED PROCESSES IN FLUIDS

A metafilm operating in the resonant state stores electromagnetic energy in the modes of the inclusions. This property can be exploited to increase the interactions experienced between the electromagnetic fields and liquids carried by the fluidic channels. There is currently an explosion of research into processes that use microwave energy to catalyze chemical or biochemical reactions[12–14] and many of these types of processes could benefit from the use of metafilms to increase the coupling between electromagnetic fields and fluids. The metafilm approach described here is particularly valuable for reactions that are implemented using a continuous flow geometry. Chemical composition can be precisely controlled by controlling reactant flow rates, while the amount of energy transferred to the fluid can be precisely controlled by controlling the frequency and power of the microwave excitation, in addition to controlling the flow rate of the fluid across the metafilm. In addition, since the resonant frequency of the metafilm array can be tailored by the geometry and arrangement of the inclusions, different metafilms with different resonant frequencies can be stimulated by a single variable-frequency source within a single waveguide.

Simulations of the electric-field strength inside the waveguide when the fundamental mode of the *S*-band waveguide is excited were conducted. For a 1-W input at 3.29 GHz the maximum field strength calculated was 8×10^2 V/m. For the same waveguide, but with the metasurface placed in

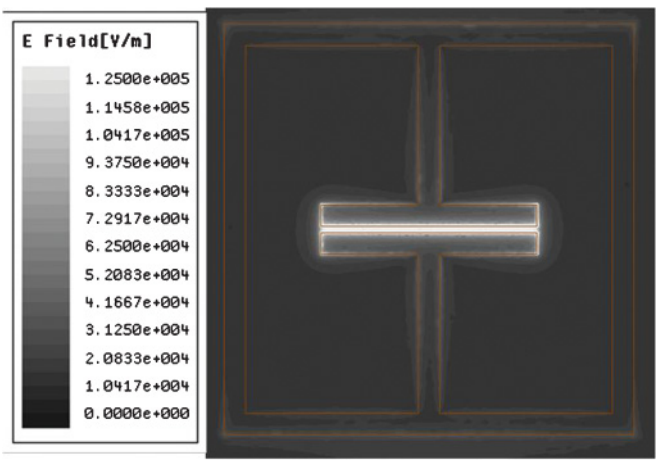

FIG. 7. (Color online) Electric-field structure in the gap of the inclusions of the metasurface showing the enhancement of the electric field. Maximum field amplitude is 1.25×10^5 V/m at 3.29 GHz.

the center, the maximum electric-field strength calculated in the gaps of the electric-field coupled inclusions was 1.25×10^5 V/m. This demonstrates a field enhancement of at least two orders of magnitude and an enhancement in the specific absorption rate (SAR) of at least four orders of magnitude. The field structure in the central gap of the inclusion is shown in Fig. 7 above.

Given that the first Floquet mode occurs when the period of the array equals $\lambda/2$, which corresponds to 13.63 GHz for this metasurface, this enhanced electric-field effect at the much lower frequency of 3.29 GHz can therefore be attributed to the unique properties of the metasurface resonance. The localized field structure shown in Fig. 7 demonstrates the possibility of using a metamaterial structure to precisely deliver electromagnetic energy. The fluid-tunable metasurface discussed above clearly demonstrates the interaction of a fluid channel with the field in the gaps of the inclusions composing the metasurface.

VI. CONCLUSION

In this paper, we numerically and experimentally demonstrated a fluid tunable metasurface fabricated from a 3×6 array of copper electric-field coupled resonators on a Duroid® substrate. Polymer tubing fluid channels were bonded to the metasurface array. Tuning over a frequency range of 150 MHz in the *S* band was achieved by flowing de-ionized water in the fluid channels. In addition to fluid tuning, the use of metasurfaces is explored for delivering electromagnetic energy for assisting in chemical processes in fluid channels. The results presented in this paper suggest that in addition to the transformation a metasurface may have on a scattered field, these highly resonant structures may have many other possible applications, including tunable resonant frequency selective surfaces, sensing and monitoring processes tied to the changes in fluid flows, as well as manufacturing, industrial, biomedical, and microwave assisted chemical processes.

[1] *Advances in Electromagnetics of Complex Media and Metamaterials*, edited by S. Zouhdi, A. Sihvola, and M. Arsalane (Kluwer Academic, Boston, 2002).

[2] N. Engheta and R. W. Ziolkowski, *Electromagnetic Metamaterials: Physics and Engineering Explorations* (Wiley-IEEE Press, 2006).

[3] G. V. Eleftheriades and K. G. Balmain, *Negative Refraction Metamaterials: Fundamental Principles and Applications* (Wiley-IEEE Press, 2005).

[4] C. L. Holloway, A. Dienstfrey, E. F. Kuester, J. F. O'Hara, and A. K. Azad, Metamaterials **3**, 100 (2009).

[5] E. F. Kuester, M. A. Mohamed, M. Piket-May, and C. L. Holloway, IEEE Trans. Antennas Propag. **51**, 2641 (2003).

[6] C. L. Holloway, D. C. Love, E. F. Kuester, A. Salandrino, and N. Engheta, IET Micr. Ant. Prop. **2**, 120 (2008).

[7] C. L. Holloway, E. F. Kuester, and D. Novotny, IEEE Antenna Wireless Propag. Lett. **8**, 525 (2009).

[8] J. A. Gordon and C. L. Holloway, IEEE Antenna Wireless Propag. Lett. **8**, 1127 (2009).

[9] A. C. Lima, E. A. Parker, and R. J. Langley, Electron. Lett. **30**, 281 (1994).

[10] W. Hu *et al.*, IEEE Microw. Wireless. Comp. Lett. **17**, 667 (2007).

[11] Meng Li, Bin Yu, and Nader Behdad, IEEE Microw and Wireless Comp. Lett. **20**, 423 (2010).

[12] B. Wathey, J. Tierney, P. Lidström, and J. Westman, Drug Discovery Today **6**, 373 (2002).

[13] C. Oliver Kappe and D. Dallinger, Nat. Rev. Drug Discovery **5**, 51 (2006).

[14] C. Fermer, P. Nilsson, and M. Larhed, Eur. J. Pharm. Sci. **18**, 129 (2002).

[15] C. L. Holloway, M. A. Mohamed, and E. F. Kuester, IEEE Trans. Electromag. Compat. **47** (2005).

[16] T. K. Wu, *Frequency Selective Surface and Grid Array* (John Wiley & Sons, New York, 1995).

[17] C. M. Soukoulis, *Photonic Band Gap Materials* (Kluwer Academic, Dordrecht, 1996).

[18] S. K. Sia and G. M. Whitesides, Electrophoresis **24**, 3563 (2003).

[19] J. Baker-Jarvis, M. D. Janezic, J. H. Grosvenor, and R. G. Geyer, NIST Technical Note 1355-R, NIST, US Department of Commerce, 1993.